Journal of Ceramic Processing Research. Vol. 27, No. 1, pp. 1~9 (2026)
(Received 16 May 2025, Received in revised form 5 September 2025, Accepted 12 September 2025)
https://doi.org/10.36410/jcpr.2026.27.1.1

J O U R N A L O F
Ceramic Processing Research

Renewable SiO_2 from fly ash for sustainable ceramic and glaze applications

Huei-Jyun Shih[a], Szu-Jung Lin[b], Ying-Chieh Lee[a,c,*] and Ting-Fu Hong[b]
[a]*Institute of Precision Electronic Components, National Sun Yat-sen University, Kaohsiung 804, Taiwan*
[b]*Department of Tropical Agriculture and International Cooperation, National Pingtung University of Science and Technology, Pingtung 91201, Taiwan*
[c]*Department of Electrical Engineering, National Sun Yat-sen University, Kaohsiung 804, Taiwan*

This study investigates the recovery and application of silica (SiO_2) from fly ash as a substitute for conventional silica in ceramic and glaze production. The microstructure analysis results reveal that the addition of quartz to fly ash facilitated the adsorption of amorphous silica onto β-quartz during calcination, leading to increased average particle size. Thermomechanical analysis indicated that the initial shrinkage temperature increased with higher quartz content due to the high thermal stability of quartz. In glaze application, substituting recycled SiO_2 for conventional silica enabled a reduction raw material while maintaining glaze adhesion and surface quality. X-ray diffraction analysis confirmed that the renewable SiO_2 successfully formed either an amorphous or microcrystalline glaze structure, depending on the formulation. Finally, regenerated SiO_2 was directly applied to ceramic teacups, exhibiting uniform coloration, excellent glaze adhesion, and a dense microstructure without significant defects, demonstrating its feasibility as a sustainable alternative in ceramics manufacturing.

Keywords: Fly ash, Renewable SiO_2, Ceramic glaze, Quartz.

Introduction

As a major energy production method, coal-fired power generation plays a crucial role in energy supply systems. However, it also produces a large amount of coal fly ash as a byproduct [1, 2]. This coal fly ash is often regarded as waste and requires proper management and disposal. However, due to limited landfill sites, population density, and strict environmental protection regulations over the globe, managing municipal solid waste is challenging due to complicated circumstances [3, 4]. Consequently, an economically feasible resolution to this issue should involve the utilization of waste materials to manufacture new products instead of resorting to land disposal. This will reduce processing costs and storage space, reaching the goal of resource recycling and sustainable management.

Coal fly ash primarily composed of silicon dioxide (45-65%) and aluminum oxide (15-30%), along with other components such as Fe_2O_3(5-15%), CaO(1-20%), MgO(1-5%), Na_2O and K_2O(0.5-5%) [5]. These characteristics make it a potential resource for various industrial applications, including road construction and building materials [1, 2]. Additionally, coal fly ashes have environmental applications, including soil improvement, wastewater treatment [6, 7], pollutant adsorption [8], zeolite [9, 10], and hybrid composite [10]. Lee et.al reported a novel development of renewable feldspar synthesized from oyster shells powder and fly ash, exhibiting a density of 2.68 g/cm^3, a compressive strength of 288 MPa [11]. Moreover, the authors found that the renewable feldspar can also be used as a bright ceramic glaze material, substituting the potash feldspar in raw material.

As a crucial element in the ceramics industry, glaze forms a dense, glassy surface that prevents liquid penetration, reducing porosity and contamination while maintaining cleanliness. However, the functionality of glazes depends largely on the materials and their compositions. The primary components of glaze include potash feldspar, quartz (SiO_2), talcum ($Mg_3Si_4O_{10}(OH)_2$), $CaCO_3$ and kaolin as well [12, 13]. These compositions and proportions influence the properties and effects of the glaze. Among them, silicon dioxide (SiO_2) is a key ingredient that provides hardness and gloss. Consequently, coal fly ash contains a considerable amount of SiO_2, it presents a potential source for modifying the structure and characteristics of glaze. However, due to the relatively low bulk density of fly ash [1], its mixing with ceramic glaze slurry can lead to phase separation [14], resulting in an uneven surface after sintering. Consequently, incorporating silicon dioxide quartz into the coal fly ash. This addition facilitates the aggregation and recrystallization of the SiO_2 content within the coal fly ash.

This study focuses on the renewable of silica from fly

*Corresponding author:
Tel : +886-7-5252-000
Fax: +886-7-5254-199
E-mail: yc56@mail.nsysu.edu.tw

ash. Due to improved grain and grain boundary diffusion, the crystalline quartz acts as a seeding material to adsorb the amorphous silica in the fly ash. This approach not only facilitates the adsorption process but also prevents phase separation caused by the low bulk density of fly ash. Additionally, the applicability of regenerated silica in glaze production is evaluated. The regenerated SiO_2 technology contributes to the renewable silica from fly ash and its substitution in ceramic glaze, thereby promoting resource recycling and sustainability. When the purity of regenerated SiO_2 can be further improved in the future, its potential applications could be significantly expanded, transforming this industrial byproduct into a valuable resource.

Materials and Methods

The coal fly ash produced by Taiwan Power Company and commercial powders of SiO_2 (99.0% purity, <33 μm, Emperor Chemical Co., Ltd) were precisely weighed according to the weight proportion of 0, 10, 20, 30, and 40% SiO_2 (named by TPC Ash-00, TPC Ash-10, TPC Ash-20, TPC Ash-30, and TPC Ash-40). Since quartz primarily serves as a nucleating agent to facilitate the adsorption of SiO_2 from fly ash, its content cannot be as low as <5%, and therefore a minimum proportion of 10% was adopted. On the other hand, the objective of this study is to promote the reutilization of SiO_2 from fly ash; hence, an excessive addition of quartz would go against the purpose of fly ash recycling. For this reason, the upper limit of quartz addition was set at approximately 40–50%. The mixture was placed in a ball mill and subjected to rolling for 8 hours. After the milling process, a 325-mesh filtration screen was used to separate the powder. The collected powder was then weighed and loaded into ceramic crucibles for calcination at 900 °C~1100 °C with a holding time of 1 hour. This thermal treatment facilitated the synthesis of renewable silica powder. After the calcination, the renewable silica powder was crushed and then passed through a 325-mesh sieve to ensure uniform particle size. Subsequently, the chemical composition of the samples was analyzed using X-ray fluorescence (XRF, Bruker S2 Ranger). X-ray diffraction (XRD) analysis with a monochromatic Cu-K_α radiation (λ = 1.540598 Å) was conducted to determine the phase composition and crystalline structure. Scanning Electron Microscope (SEM, JOEL–7600 F) with an acceleration voltage of 10 kV, along with energy-dispersive spectroscopy (EDS) was carried out to capture microstructure. The thermal expansion was measured using a Thermal Mechanical Analyzer (TMA, SHIMADZU, TMA-60) up to 1300 °C. In the glaze experiments, the commercial powders (Emperor Chemical Co., Ltd) of $CaCO_3$ (98.0% purity, 1.93 μm), Fe_2O_3 (96.0% purity, <5 μm), CuO (98.0% purity, <10 μm), K-feldspar (99.0% purity, <10 μm) were mixed with different compositions of renewable silica, de-ionized water and 0.2 wt% dispersant (Dispex AA4040, Tye Han Trading Co., Ltd). The aqueous solution was evenly coated onto an alumina substrate using an adjustable coater to control the thickness of the glaze precursor layer. The coated samples were then placed in a furnace for sintering at 1200 °C for 20 minutes to form the final glazed surface. After sintering, the glaze gloss was measured using a gloss meter, while surface roughness was assessed with a surface profilometer to establish the correlation between gloss values and surface roughness. Additionally, an optical microscope (OM) was employed to examine the crystallization behavior of the glaze surface. SEM and XRD were also used to characterize the microstructure and crystalline.

Result and Discussion

Table 1 presents the XRF analysis results for TPC Ash-10 and TPC Ash-20 following calcination. As reported in a previous study [11], the chemical compositions of both samples closely resemble that of conventional coal fly ash. The addition of quartz primarily results in an increased concentration of silicon dioxide (SiO_2), while the concentrations of other major oxides—such as aluminum oxide (Al_2O_3), iron oxide (Fe_2O_3), calcium oxide (CaO), potassium oxide (K_2O), and titanium dioxide (TiO_2)—remain largely unchanged. These findings indicate that the fundamental chemical characteristics of the fly ash are retained, with the observed variations primarily attributable to the externally introduced quartz.

Figure 1 shows the XRD patterns of different quartz composition in coal fly ash calcined from 900 °C to 1100 °C. In general, calcination temperatures are chosen within 0.5–0.8 of the melting point (K) of the target material, which ensures sufficient solid-state diffusion to enable decomposition, phase transformation, or crystallization [15, 16]. Consequently, since fly ash is mainly composed of SiO_2 (melting point 1743 K) and Al_2O_3 (melting point 2345 K), the calcination temperature was deliberately selected in the range of 900–1000 °C. This range allows adequate reactivity for silica to agglomerate, while avoiding excessively high temperatures that could

Table 1. XRF analysis for TPC Ash-10 and TPC Ash-20.

	SiO_2	Al_2O_3	Fe_2O_3	CaO	MgO	K_2O	TiO_2	Na_2O	P_2O_5	Total
TPC Ash-10	64.79	23.52	4.85	1.96	1.22	1.31	1.05	0.95	0.35	100%
TPC Ash-20	72.83	18.76	3.03	1.58	0.98	1.02	0.81	0.73	0.26	100%

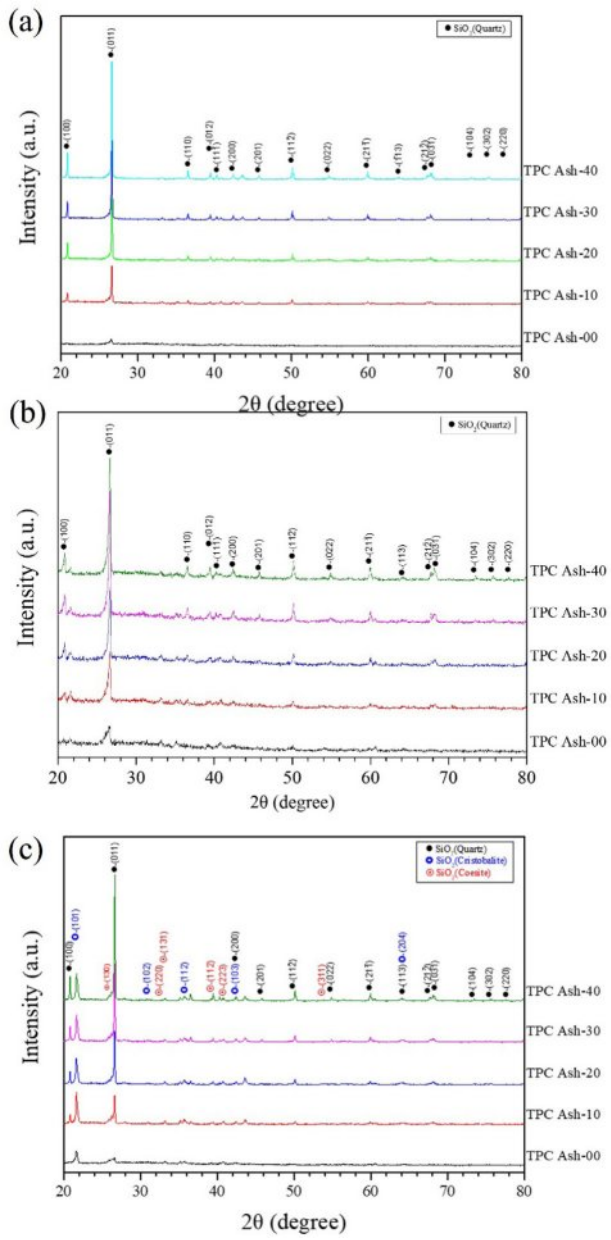

Fig. 1. X-ray diffraction patterns of coal fly ash with 0% to 40% of quartz calcinated at (a) 900 ℃ (b) 1000 ℃ (c) 1100 ℃.

trigger unwanted reactions of alumina. After calcination, pure coal fly ash did not exhibit any significant phase transformation, the primary phase probably corresponds to a weak α-quartz phase (SiO_2, JCPDS Card No. 78-2315). However, the primary structure of silicon dioxide in the coal fly ash were still considered to be amorphous for all the calcination temperature. Upon the addition of 10%, silicon dioxide α-quartz becomes the dominant phase, this is attributed to the addition of 10% quartz. Furthermore, it was observed that the intensity of the quartz phase increased proportionally with the added quartz content from TPC Ash-10 to TPC Ash-40. The phase structures were compared with the Powder Diffraction Database, confirming that all the samples primarily exhibit the pure α-quartz phase, adopting a hexagonal crystal system (space group $P6_421$ or $P6_221$). According to the phase diagram of SiO_2 [17], quartz exists as β-quartz phase at high temperatures and transforms to α-quartz at room temperature. Consequently, most of all samples exhibit the same single quartz phase at 900 ℃ and 1000 ℃ as shown in Fig. 1(a) and 1(b). However, when calcination temperature raises to 1100 ℃, some secondary phases can be found in the patterns due to phase transition at high temperature, such as cristobalite (JCPD cards No.82-0512) and coesite (JCPD cards No.77-1726), as shown in Fig. 1(c).

Figure 2 compares the XRD patterns of coal fly ash containing 20% quartz before and after calcination at 1000 ℃. It can be observed that both pre-calcined and post-calcined TPC Ash-20 exhibit a α-quartz phase structure (JCPDS Card No. 85-0504). However, the full width at half maximum (FWHM) of the (011) plane in TPC Ash-20 was determined to be 0.142°, whereas that of quartz-adsorbed TPC Ash-20 increased to 0.202°. The broadening of the XRD peak indicates a decrease in crystallinity. Furthermore, the relative intensity of the quartz (100) plane compared to quartz (011) plane also increased from 23.6% to 31.1% after adsorption, this indicates that as silica gradually adsorbs onto quartz, the anisotropy between the various crystal planes decrease. These results suggest that calcination effectively promotes the adsorption of amorphous silica from fly ash onto quartz, thereby deteriorating the crystallinity as reflected by the increased FWHM. This indicates that calcination successfully facilitates the adsorption of amorphous silica from fly ash onto quartz, thereby reducing the X-ray diffraction intensity. Additionally, the broadening of diffraction peaks suggests that the adsorbed amorphous silica gradually establishes crystallographic relationships with α-quartz during the adsorption, grain boundary diffusion, and recrystallization processes [18, 19]. This observation will be further corroborated by SEM analysis.

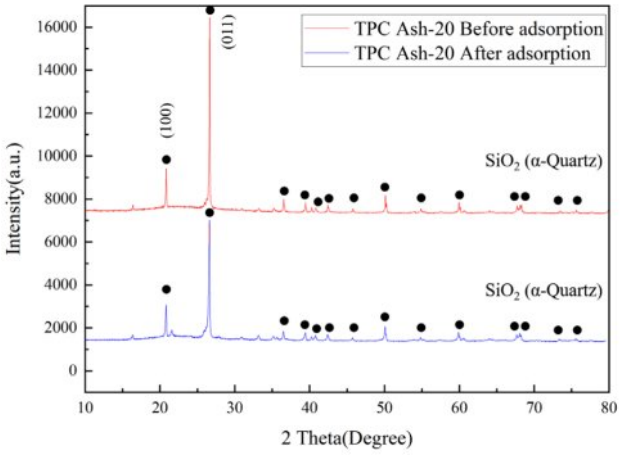

Fig. 2. X-ray diffraction patterns of coal fly ash with 20% quartz before adsorption.

Figure 3 presents the laser particle size analysis results of the calcined powders, providing further evidence of the adsorption effect of quartz. The particle size analyzer measurements confirm that the average particle size (D50) of the powders exhibits a continuous aggregation trend with increasing calcination temperature. A comparison between the samples containing quartz and TPC Ash-00 (without quartz) reveals distinct differences in particle size evolution with increasing temperature. At a sintering temperature of 900 °C, the average particle size gradually develops a bimodal distribution with increasing quartz content, as shown in Fig. 3(a). When the sintering temperature reaches 1000 °C, the fraction of fine particles decreases significantly, forming larger aggregated particles. At 1100 °C, this trend continues, with the fine particle fraction further decreasing and the proportion of larger particles increasing as shown in Fig. 3(c). Besides, as the arrow pointing, the beginning point of distribution peak also increase from 5 μm to 7 μm from 1000 °C to 1100 °C, making the peak narrow and move to larger size distribution. These results indicate that the addition of quartz significantly enhances the temperature-dependent growth in average particle size [20, 21]. Moreover, for TPC Ash-00, the D50 increased from 9.35 μm at 900 °C to 14.33 μm at 1000 °C, but remained relatively stable at 14.46 μm at 1100 °C as shown in Fig. 3(d). In contrast, for TPC Ash-20, the D50 increased from 10.32 μm at 900 °C to 14.32 μm at 1000 °C, and further increased to 18.60 μm at 1100 °C. Furthermore, when the quartz addition was increased to 30% and 40%, the average particle size D50 at 1100 °C increased to 18.94 μm and 19.18 μm, respectively. This suggests that the initially stable fly ash particles, upon the introduction of SiO_2, become more prone to adhesion onto the quartz surface due to thermal effects, leading to an increase in the overall particle size [22, 23]. A similar trend can also be observed in the particle size distribution of D10. Consequently, the aggregation effect in coal fly ash with added quartz becomes more pronounced at high temperature.

Figure 4(a)–4(e) presents the SEM images of TPC-Ash 00, TPC-Ash 10, TPC-Ash 20, TPC-Ash 30, and TPC-Ash 40. The SEM analysis of fly ash samples with added quartz revealed a microstructure characterized by spherical or irregularly distributed particles. Consistent with the results of particle size analysis, varying the proportion of added silica did not lead to significant differences in the particle size distribution of the regenerated silica powder. However, a noteworthy observation is that in samples containing quartz, numerous finer silica particles were found to be adsorbed onto the surfaces of larger silica grains, as shown in Fig. 4(f). This suggests that quartz promotes the aggregation of finer silica particles, likely through enhanced surface interactions and diffusion effects at elevated temperatures [24, 25]. Additionally, in samples with a higher quartz content, larger particles exhibited more pronounced adhesion of smaller particles, indicating that quartz plays a crucial role in facilitating particle coalescence and stabilization during thermal processing.

Therefore, the process of utilizing silicon dioxide (quartz) as a seeding agent to adsorb amorphous

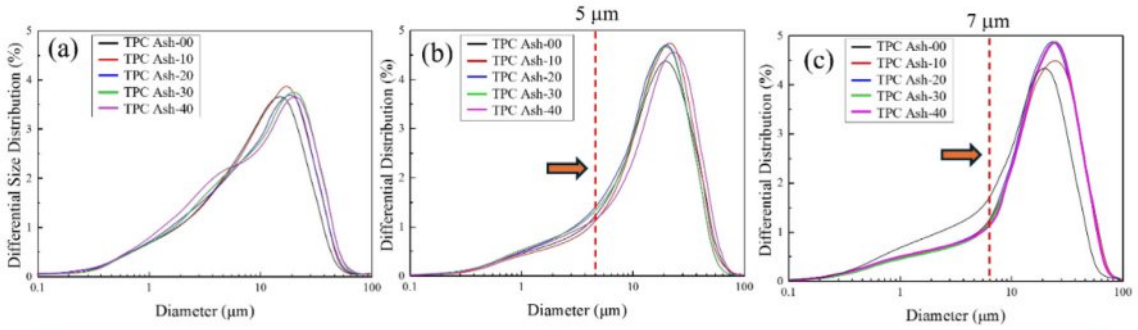

(d)

Particle Size D10 (μm)					
	TPC Ash-00	TPC Ash-10	TPC Ash-20	TPC Ash-30	TPC Ash-40
900 °C	1.39	1.58	1.48	1.46	1.50
1000 °C	2.20	2.26	1.99	2.01	2.13
1100 °C	1.77	2.70	2.66	2.74	2.59
Particle Size D50 (μm)					
	TPC Ash-00	TPC Ash-10	TPC Ash-20	TPC Ash-30	TPC Ash-40
900 °C	9.35	10.32	10.21	9.99	9.32
1000 °C	14.33	14.32	13.32	14.01	15.40
1100 °C	14.46	18.60	17.96	18.94	19.18

Fig. 3. Particle size distribution for renewable silicon dioxide calcinated at (a) 900 °C (b) 1000 °C (c) 1100 °C and (d) D10, D50 particle size.

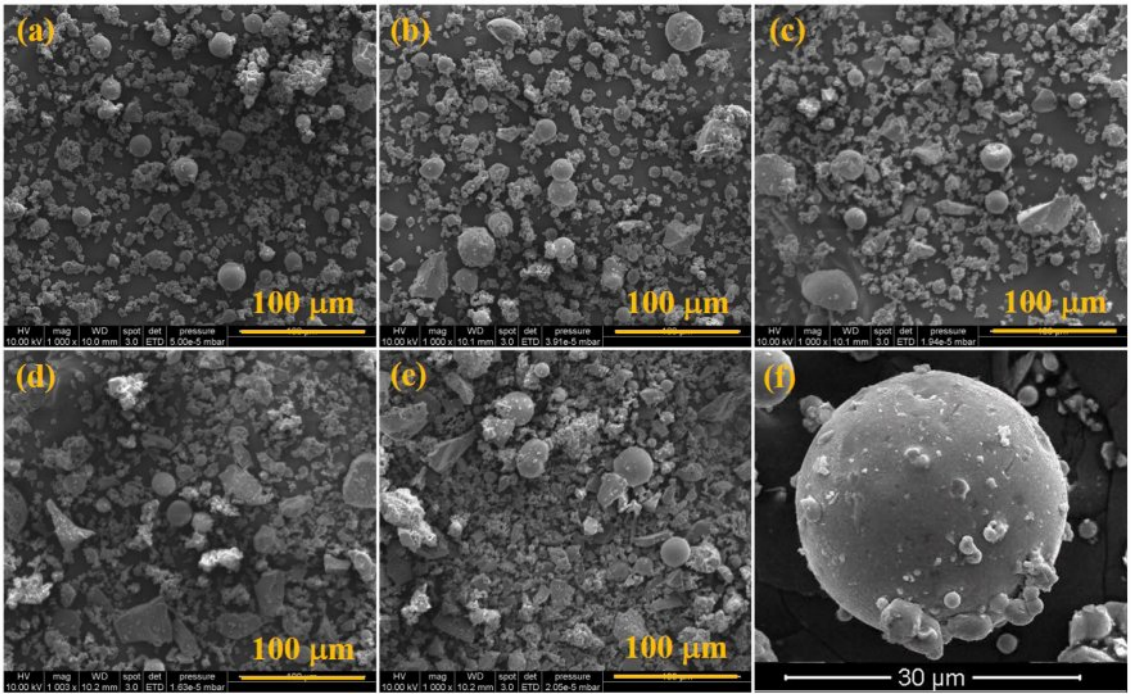

Fig. 4. SEM images for coal fly ash with various compositions of quartz calcinated at 1000 °C (a) 0%, (b) 10%, (c) 20%, (d) 30%, (e) 40% quartz, and (f) enlarged view of adhesion quartz particle.

silica from fly ash is schematically illustrated in Fig. 5. Initially, quartz (SiO_2) is thoroughly mixed with various constituents of fly ash—including SiO_2, Al_2O_3, MgO, K_2O, Na_2O, and Fe_2O_3—via ball milling to ensure homogeneity. Although the XRF results indicate the possible presence of other minor constituents in the fly ash. However, after mixing the fly ash with quartz, the proportion of these minor components is further reduced. Moreover, XRD analysis reveals no distinct peaks corresponding to these secondary phases, suggesting that their quantities are minimal or that they exist in microcrystalline and even amorphous. Therefore, it can

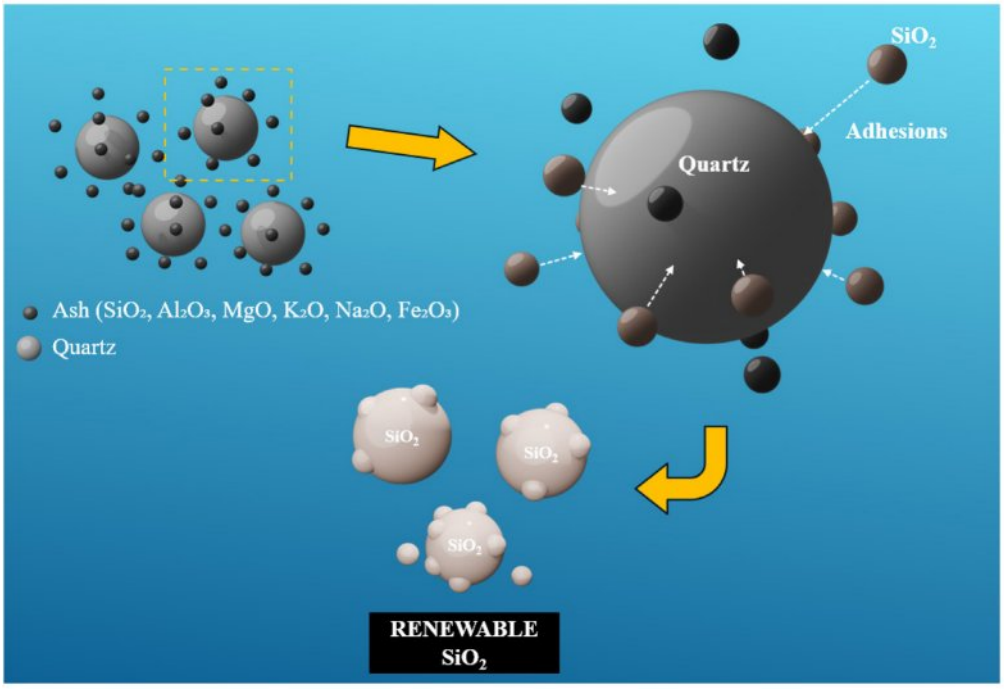

Fig. 5. Schematic for the amorphous SiO_2 adhesions process on the surface of quartz.

be inferred that the primary species adsorbed onto the quartz particles is silica. Upon subjecting the well-mixed powders to high-temperature calcination, the thermal energy facilitates significant mass transport phenomena. Given that silica is the predominant component in fly ash, a considerable portion of amorphous SiO_2 tends to migrate and adsorb onto the surface of the added quartz particles. Additionally, the melting points of Al_2O_3 (2072 °C), CaO (2570 °C), and Fe_2O_3 (1565 °C) are significantly higher than that of SiO_2 (1470 °C). Under the calcination employed (900–1100 °C), these oxides lack sufficient thermal energy to facilitate grain or grain boundary diffusion like SiO_2 [16]. A further consideration is that quartz and silica are isomers, which results in stronger interfacial bonding compared to the heterogeneous interfaces between silica and other oxides [26, 27]. Consequently, silica exhibits a greater tendency to adsorb onto quartz particles relative to other impurities. This preferential adsorption is attributed to the relatively higher diffusion rate of silica compared to other oxides. Consequently, this process promotes the growth of larger silica domains, thereby enabling the selective separation of silica from other inorganic components within the fly ash matrix. Ultimately, this approach enhances the efficiency of silica recovery and purification from coal-derived waste materials.

To investigate the sintering characteristics of coal fly ash with 0%, 10%, 20%, 30%, and 40% quartz content, we performed thermomechanical analysis (TMA) on the calcined regenerated SiO_2 using a thermal analyzer. During the preparation of test specimens, due to the lack of adhesion in the calcined powder, polyvinyl alcohol (PVA) was added to form tablet-shaped samples. According to the TMA results in Fig. 6, all renewable SiO_2 samples exhibited a slightly expansion point at approximately 537°C, which is inferred to correspond to the α-quartz to β-quartz phase transition [28, 29]. When the temperature exceeds 1250 °C, the specimens exhibit significant length shrinkage, which is attributed to the onset of densification as the material approaches its melting point [30]. This phenomenon is referred to as the initial shrinkage temperature. Furthermore, it is observed that the initial shrinkage temperature increases with the addition of quartz. This is attributed to high β-quartz SiO_2 content in TPC Ash-40, which prevents significant shrinkage, thus inhibiting noticeable shrinkage [30, 31]. Compared to β-quartz, which has a high melting point (~1700 °C) [32], fly ash primarily consists of amorphous silica (approximately 60%) and alumina (around 30%) [11, 33]. Due to the lower melting points of these components relative to β-quartz, the overall melting behavior of fly ash is significantly different. As the proportion of β-quartz increases, the initial shrinkage temperature also rises. This can be attributed to the thermal stability of β-quartz at high temperature, which impedes the densification process at lower temperatures, thereby delaying the onset of sintering and structural

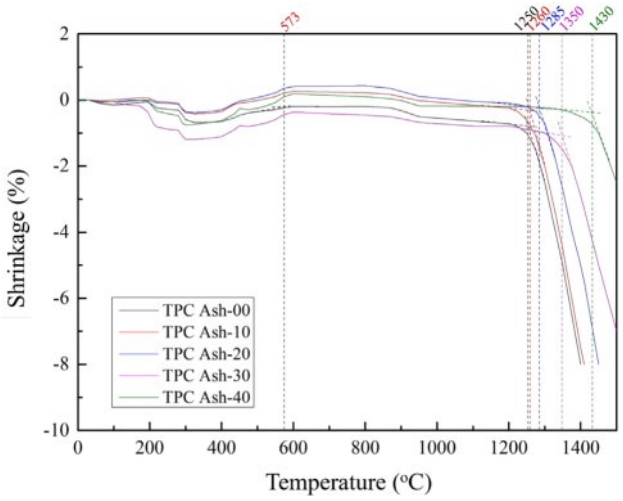

Fig. 6. Thermomechanical analysis for the pellets of calcined coal fly ash with 0 to 40% quartz.

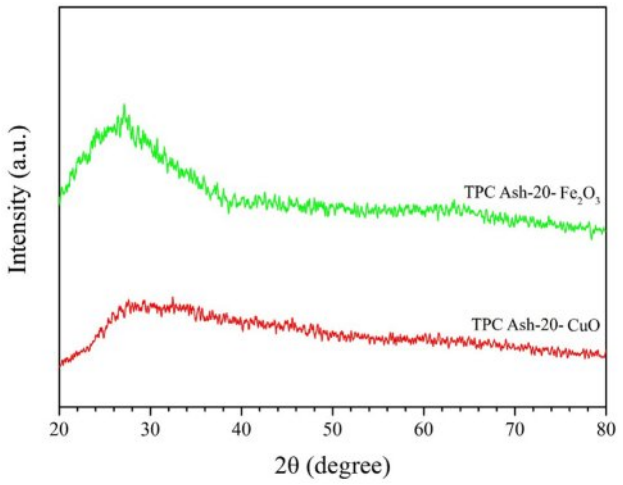

Fig. 7. X-ray diffraction patterns for renewable silica (TPC Ash-10) ceramic glaze with different chromophores.

shrinkage.

On the application of glaze experiment, a ceramic glaze formulation was prepared using 50% K-feldspar, 25% quartz, 10% talc ($Mg_3Si_4O_{10}(OH)_2$), 10% $CaCO_3$ (calcium carbonate), and 5% kaolin [34]. In this formulation, 25% quartz was replaced with renewable silica (TPC Ash-10). Mattia Sisti et al. have experimented with various formulations of ceramic glazes, incorporating between 40 % and 50 wt% of this glassy material [35]. The most promising formulation involves 44 wt% of waste, resulting in a shiny, dark ceramic glaze. This demonstrates that many waste materials have significant potential for recycling and reuse. Here we use two different chromophores were incorporated: 2% CuO and 5% Fe_2O_3 [36]. The glaze samples were sintered at 1200 °C. As shown in Fig. 7, the XRD analysis of the final sintered ceramic glaze confirms that, under the influence of sintering aids, the glaze successfully formed

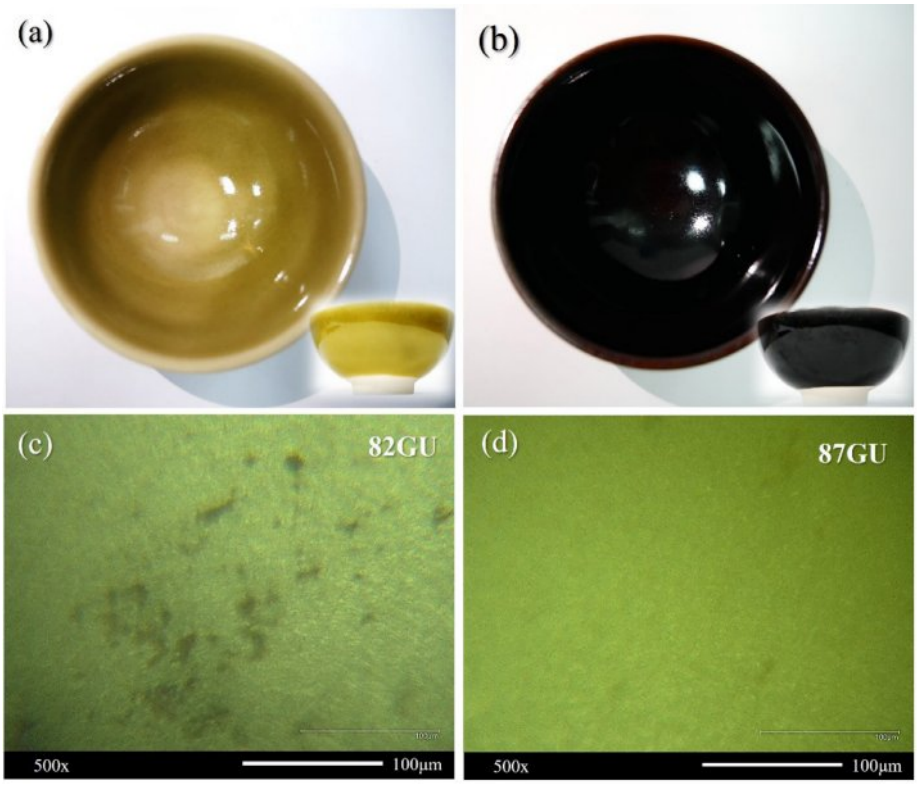

Fig. 8. (a) Digital pictures for renewable silica (TPC Ash-10) ceramic glaze with CuO and (b) Fe_2O_3 chromophores. (c) Optical images for renewable glaze with CuO and (d) Fe_2O_3 chromophores.

an amorphous glassy phase at 1200 °C [37]. According to the study of Sundari, K. N. et al. [38], coesite is a high-temperature polymorph of quartz with a relatively low thermal expansion coefficient, which can improve the thermal stability and heat resistance of glazes. Its presence helps to reduce thermal cracking while enhancing the strength and texture of the glaze surface. Cristobalite, on the other hand, is a high-temperature, high-pressure phase of SiO_2 [39], that is less commonly applied in glaze formulations. Since both of these secondary phases typically form at elevated temperatures (around 1100 °C), their appearance can be effectively avoided by carefully controlling the calcination temperature, thereby minimizing their potential influence on glaze performance.

Figures 8(a)–(b) present optical images of ceramic teacups colored with CuO and Fe_2O_3, respectively. The results indicate that the glaze exhibited no visible surface defects, with uniform adhesion and even color distribution, without noticeable variations. Additionally, no glaze accumulation or flow was observed at the lower edges of the cups. However, these microstructural characteristics had minimal impact on the glossiness of the glaze, as the measured gloss values remained above 80 GU, as shown in Fig. 8(d). Optical microscopy analysis of the glaze surface revealed fine crystalline grains in CuO samples, while Fe_2O_3 samples exhibited both fine grains and minor mottling [40, 41].

Figures 9(a) and (b) show the SEM surface morphology for CuO glaze and Fe_2O_3 glaze adopted recycled SiO_2. CuO glaze with recycled SiO_2 shows some nano-crystal on the surface and CuO glaze with recycled SiO_2 present some micro-structure. But basically, there

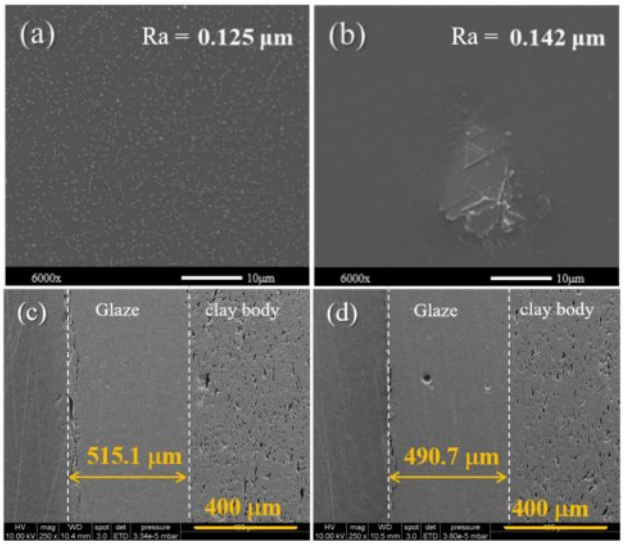

Fig. 9. (a) Surface morphology for renewable silica (TPC Ash-10) ceramic glaze with CuO and (b) Fe_2O_3 chromophores. (c) Cross-section views for renewable silica (TPC Ash-10) ceramic glaze with CuO and (d) Fe_2O_3 chromophores.

does not affect the surface roughness much. Besides, the surface roughness for CuO samples and Fe_2O_3 samples were 0.125 and 0.142 um. According to the literature [42], achieving the glossy appearance characteristic of ceramic glazes generally requires a surface roughness in the range of Ra 0.2–0.4 μm. Accordingly, the present results demonstrate that glassy phases of copper oxide and iron oxide ceramic glazes can be effectively mixed with recycled silica, yielding low surface roughness and thereby producing a favorable visual effect. SEM images in Figs. 9(c) and (d) revealed that, although the CuO-based formulation exhibited some residual bubbles, both formulations achieved a dense, pore-free cross-sectional structure at the optimized sintering temperature. Additionally, a well-bonded interface between the glaze layer and the ceramic body was observed. The measured glaze thicknesses were 515 μm and 490 μm, respectively. These results indicate that regenerated SiO_2 can successfully replace quartz in ceramic glaze formulations.

Conclusion

This study investigates the recovery and application of silica (SiO_2) from fly ash as a substitute for conventional silica in ceramic and glaze production. XRD analysis confirmed that the addition of quartz to fly ash facilitated the adsorption of amorphous silica onto β-quartz during calcination at high temperatures, leading to increased particle aggregation and crystallographic alignment. Particle size analysis demonstrated that increasing quartz content promoted the growth of larger silica particles through thermal effects. SEM images further confirmed the enhanced adhesion of fine silica particles onto quartz surfaces, highlighting quartz's role in particle coalescence. Thermomechanical analysis indicated that the initial shrinkage temperature increased with higher quartz content due to the high thermal stability of quartz. In glaze application, substituting recycled SiO_2 for conventional silica enabled a reduction in sintering temperature from 1200 °C to 1150 °C while maintaining glaze adhesion and surface quality. XRD analysis confirmed that the regenerated SiO_2 successfully formed either an amorphous or microcrystalline glaze structure, depending on the formulation. Finally, regenerated SiO_2 was directly applied to ceramic teacups, exhibiting uniform coloration, excellent glaze adhesion, and a dense microstructure without significant defects, demonstrating its feasibility as a sustainable alternative in ceramics manufacturing.

Declaration of Interest Statement

The authors declare that they have no known competing financial interests or personal relationships that could have appeared to influence the work reported in this paper.

Funding

This work was supported by the National Science and Technology Council (NSTC), Taiwan through grant number 111-2221-E-110 -064 -MY3 and 113-2221-E-110 -015 -MY3

References

1. M. Ahmaruzzaman, Prog. Energy Combust. Sci. 36[3] (2010) 327-363.
2. B.A. Tayeh, H.M. Hamada, I. Almeshal, and B.A. Bakar, Case Stud. Constr. Mater. 17 (2022) e01429.
3. Y.C. Lee, A.O. Nurlatifah, H.J. Shih, and E. Widyastuti, J. Mater. Cycles Waste Manag. 27 (2025) 1394-1405.
4. H.J. Shih, Y.C. Lee, J.R. Pan, and C. Chung, Anti-Corros. Methods Mater. 72[1] (2025) 61-70.
5. F. Teng, Z. Wang, K. Ren, S. Liu, and H. Ding, J. Environ. Manage. 357 (2024) 120783.
6. H. Wu, Y. Zhu, S. Bian, J.H. Ko, S.F.Y. Li, and Q. Xu, Chemosphere 195 (2018) 40-47.
7. J. Tang, M. Su, Q. Wu, L. Wei, N. Wang, E. Xiao, H. Zhang, Y. Wei, Y. Liu, C. Ekberg, B.M. Steenari, and T. Xiao, J. Clean. Prod. 234 (2019) 139-149.
8. Q. Qiu, X. Jiang, G. Lv, Z. Chen, S. Lu, M. Ni, J. Yan, and X. Deng, Powder Technol. 335 (2018) 156-163.
9. N. Koshy and D. N. Singh, J. Environ. Chem. Eng. 4[2] (2016) 1460-1472.
10. B.R.N. Murthy, A.M. Ambekar, and A. Hiremath, J. Compos. Sci. 8[3] (2024) 90.
11. Y.C. Lee, H.J. Shih, and E. Widyastuti, Ceram. Int. 51 (2025) 23124-23132.
12. Z. Sarnecka, C. Mazzocchi, A. Chwalik, E. Musialik, M. Pisulińska, E.K. Świetlicka, J. Tarasiuk, M. Wachowiak, and L. Bonizzoni, Archaeometry 67[4] (2025) 984-1000.
13. M. Yuan, J. Hou, X. Zhang, N. Wood, J. Molera, H. Castillo-Michel, M. Cotte, and T. Pradell, J. Am. Ceram. Soc. 107[11] (2024) 7577-7593.
14. H. Yang, H. Guo, H. Sun, and T. Peng. Molecules 29[16] (2024) 3740.
15. Y.C. Lee, H.J. Hsu, I.Y. Huang, H.J. Shih, and C. Pithan, J. Ceram. Process. Res. 24[6] (2023) 992-1000.
16. A. Iles, F. Zaoui, B. Elhadj Daouadji, M.A. Zorgani, L. A. Siddig, A.S. Abdelhamid, S. Abubakar, B. Bounaceur, E. Choukchou-Braham, F. Lebsir, and N. Saleh, J. Water Process Eng. 66 (2024) 105960.
17. G.M. Lo Piccolo, M. Cannas, and S. Agnello, Materials 14[24] (2021) 7682.
18. S. Bates, G. Zografi, D. Engers, K. Morris, K. Crowley, and A. Newman, Pharm. Res. 23 (2006) 2333-2349.
19. N. Chanka, W. Donphai, M. Chareonpanich, K. Faungnawakij, G. Rupprechter, and A. Seubsai, ACS Omega 9[6] (2024) 6749-6760.
20. P. Kalita, R. Parveen, S. Ghosh, V. Grover, Y.K. Mishra, and D.K. Avasthi, J. Alloys Compd. 1012 (2025) 178330.
21. D. Pérez-Coll, P. Núñez, and J.R. Frade, J. Power Sources 196[20] (2011) 8383-8390.
22. S. Ahmed and M.S. Vohra, Chem. Eng. J. 500 (2024) 156525.
23. A.G. Meskel, M.M. Kwikima, B.T. Meshesha, N.G. Habtu, S.C.S. Naik, and B.P. Vellanki, Environ. Challenges 14 (2024) 100829.
24. H.J. Shih, Y.C. Lee, and C.T. Yang, Open Ceram. 19 (2024) 100635.

25. Y.C. Lee, H.J. Shih, T.Y. Wang, and C. Pithan, J. Eur. Ceram. Soc. 44[10] (2024) 5659-5667.
26. A.M. Schrader, J.I. Monroe, R. Sheil, H.A. Dobbs, T.J. Keller, Y. Li, S. Jain, M.S. Shell, J.N. Israelachvili, and S. Han, Proc. Natl. Acad. Sci. U.S.A. 115[12] (2018) 2890-2895.
27. C.Y. Kim and S.C. Yi, J. Ceram. Process. Res. 10[4] (2009) 462-468.
28. J.D. Axe and G. Shirane, Phys. Rev. B 1[1] (1970) 342.
29. I. Ohno, K. Harada, and C. Yoshitomi, Phys. Chem. Miner. 33 (2006) 1-9.
30. V.T. Trinh, B.H. Lee, and C.H. Jeon, J. Ind. Eng. Chem. 131 (2024) 481-489.
31. T. Okuizumi, G. Horiguchi, H. Kamiya, and Y. Okada, Energy Fuels 38[3] (2024) 2319-2326.
32. H. Gao, G. Li, and Z. Zhang, PEPS 11[1] (2024) 20.
33. L. Puri, Y. Hu, and G. Naterer, Front. Fuels 2 (2024) 1378361.
34. R. Casasola, J.M. Rincón, and M. Romero, J. Mater. Sci. 47 (2012) 553-582.
35. M. Sisti, D. Guidetti, F. Altimari, F. Andreola, L. Barbieri, I. Lancellotti, L. Casini, F. Colombo, R. Arletti, R. Fantini, and A.F. Gualtieri, Ceram. Int. 51[4] (2025) 4195-4205.
36. I. Peng, K. Hills-Kimball, I.M. Lovelace, J. Wang, M. Rios, O. Chen, and L. Q. Wang, Colorants 1[4] (2022) 376-387.
37. M.G. Rasteiro, T. Gassman, R. Santos, and E. Antunes, Ceram. Int. 33[3] (2007) 345-354.
38. K.N. Sundari, D.C. Birawidha, H. Prasetia, I.W. Mudra, and Y. Hendronursito, Physicochem. Probl. Miner. Process. (2024) 60.
39. N. Zeren and S. Abalı, J. Ceram. Process. Res. (2025) 231-238.
40. R.A. Platova and Y.T. Platov, Glass Ceram. 74 (2017) 91-94.
41. M. Safi, N. Khalili, and A. M. Arabi, JCST 5[4] (2011) 253-261.
42. J.S. Kim, U.S. Kim, J.H. Choi, J.H. Kim, and K.S. Han, J. Ceram. Process. Res. 25[1] (2024) 65-71.